RSC Advances

ROYAL SOCIETY OF CHEMISTRY

www.rsc.org/advances

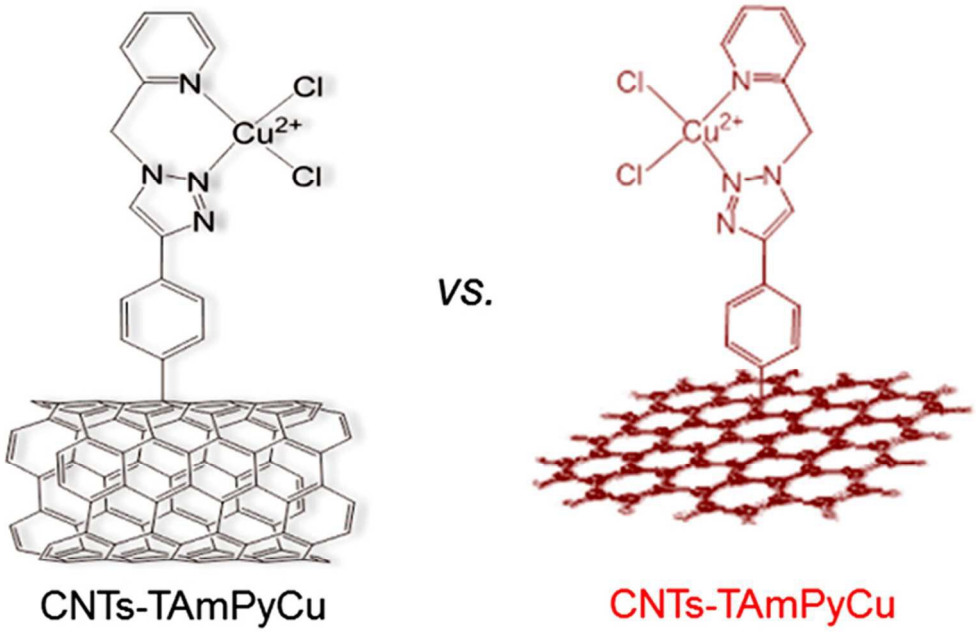

graphical abstract
75x50mm (300 x 300 DPI)

Journal Name

RSCPublishing

ARTICLE

Copper Complex Covalently Grafted on Carbon Nanotubes and Reduced Graphene Oxide Promotes Oxygen Reduction Reaction Activity and Catalyst Stability

Cite this: DOI: 10.1039/xoxxoooooox

Received ooth January 2012,
Accepted ooth January 2012

DOI: 10.1039/xoxxoooooox

www.rsc.org/

Ru-Chun Wang,[a] Tian-Liang Yin,[a] Ping-Jie Wei,[a] and Jin-Gang Liu[a *]

Developing new non-precious-metal catalysts for oxygen reduction reaction (ORR) is very important to the final substitution of a platinum-based noble metal catalyst for large-scale commercialization of fuel cells. Herein, we report two new composites CNTs-TAmPyCu and rGO-TAmPyCu as ORR electrocatalysts, where a triazole-pyridine coordinated copper complex TAmPyCu was covalently grafted onto multi-walled carbon nanotubes (CNTs) and reduced graphene oxide (rGO), respectively. Covalent immobilization of a copper complex on CNTs or rGO remarkably improves the catalyst ORR activity and stability compared with that of the physisorbed counterparts. Furthermore, the rGO-TAmPyCu composite significantly enhanced the selectivity of $4e^-$ versus $2e^-$ reduction of O_2 relative to the CNTs-TAmPyCu catalyst, suggesting the beneficial effect of the flat rGO as supporting material for copper complexes. The ORR activity of the rGO-TAmPyCu catalyst was also compared with a reported multi-nuclear copper assembly. The results from this study suggest that creating more proximal dinuclear Cu sites on supporting is an effective approach to promote the oxygen $4e^-$ reduction process, and a multinuclear Cu assembly is crucial for efficient O_2 reduction with impressively lowered overpotential.

Introduction

The oxygen reduction reaction (ORR) is a very important process, not only in various biochemical transformations, but also in energy conversion systems such as fuel cells and air-batteries.[1-3] The sluggish nature of ORR kinetics at the cathode is one of the key barriers for hydrogen–oxygen fuel cells. The noble metal Pt is now predominantly used as an ORR catalyst in fuel cells. However, its mass application is limited by high costs and scarce reserves.[4-5] Moreover, the Pt catalyst suffers from issues of stability, susceptibility towards CO poisoning, and apparent methanol crossover effects. As a potential replacement for Pt, non-precious-metal catalysts (NPMCs) have attracted considerable research attention in recent years. Several types of NPMCs have been investigated, including transition metal macrocyclic compounds, carbon-supported transition metal complexes of nitrogen-containing ligands (M-N/C; normally, M = Fe or Co), chalcogenides, biological enzymes, and bio-inspired compounds.[6-8] Among the NPMCs studied, M-N/C catalysts have been investigated most intensively. Traditionally, these have been prepared by pyrolysis with carbon, a nitrogen-containing precursor, and metal salt at high temperatures. Two recent nice examples of M-N/C catalysts have demonstrated their possible competence in performing as a state-of-the-art Pt/C catalyst.[9, 10] Nevertheless, the pyrolysis treatment destroyed the original chemical structures of the precursors. As a result, the ORR active sites and the related catalytic mechanism remain elusive, which makes it difficult to tailor the structure and surface properties of the catalysts.[11] It remains a great challenge to replace Pt-based catalysts with NPMCs while maintaining comparable performance in practical applications.

Copper ions are involved in various bio-transformations, and copper-containing enzymes such as laccase catalyze the four-electron reduction of O_2 to H_2O very efficiently with almost no overpotential (20 mV).[8,12] Because of their biological relevance, various copper-based catalysts and their ORR activities have been investigated electrochemically.[13] Copper macrocycles such as porphyrins and phthalocyanines have exhibited both limited activity towards ORR and poor stability. Copper complexes with amino-alkyl ligands have demonstrated ORR activity with relatively negative onset potentials in neutral solutions.[14] Copper complexes with 1, 10-phenanthroline and its derivatives have shown good ORR activity, and it has been suggested that the electroreduction of O_2 proceeds via a binuclear $[Cu_2O_2]$ intermediate.[15-18] A triazole copper compound [Cu(Hdatrz)] supported on carbon black was found to be one of the most efficient synthetic copper electrocatalysts for the ORR with an onset potential of 0.86 V (vs. RHE) at pH 13.[19] Despite its good ORR activity, this copper catalyst showed very poor long-term stability in basic solutions.[20] The aforementioned Cu ORR catalysts, prepared without pyrolysis treatment, have the advantage that their ORR activity is tunable through tailoring the structure of the coordinated ligands. However, this kind of catalyst suffers from very low stability,

partly due to poor electron transfer from the support to the catalyst.

The covalent immobilization of ORR catalysts on supporting materials might benefit from the facile electron transfer between the catalyst and the support, as well as holding the catalyst tightly without detaching. We recently developed a bio-inspired ORR catalyst in which a biomimetic heme model compound was covalently grafted onto the support of carbon nanotubes (CNTs), which showed both superior ORR activity and stability to that of commercial Pt/C catalysts.[21] A multi-nuclear copper assembly, a mimic of the active site of laccase, was also immobilized on the surface of reduced graphene oxide (rGO) via the covalent grafted triazole-dipyridine dinucleating ligand. The bio-inspired copper catalyst exhibits high ORR activity, and superior long-term stability to commercial Pt/C catalyst in alkaline media.[22] In this work, a triazole-pyridine coordinated copper complex (TAmPyCu) was covalently grafted onto multi-walled CNTs and rGO, producing composite of CNTs-TAmPyCu and rGO-TAmPyCu as new ORR catalysts, respectively (Fig. 1). The purpose of this study is to investigate the effect of different supporting materials (rGO vs. CNTs), and different immobilization methods (physisorbebd vs. covalent grafting) of the catalysts on the corresponding ORR performance.

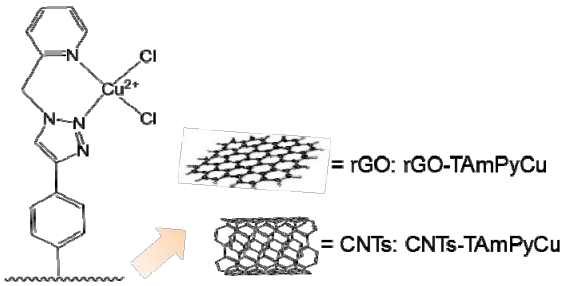

Figure 1 Schematic representation of the rGO/CNTs-TAmPyCu composites.

Experimental

Chemicals.

All reagents were purchased commercially and used without further purification unless otherwise noted. GO was obtained by harsh oxidation of the graphite powder according to the modified Hummers method.[23, 24] MWCNTs (length 50 μm, OD 8–15 nm, ID 3–5 nm) were obtained from Chengdu Organic Chemical Co. Ltd, Chinese Academy of Sciences. 4-((triisopropylsilyl)ethynyl) benzene-diazonium tetrafluoroborate,[25] 2-(azidomethyl)pyridine, [26] 2-((4-phenyl-1H-1,2,3-triazol-1-yl)methyl)pyridine (TAmPy) and TAmPyCu [27] were prepared according to the literature.

Synthesis of the CNTs-TAmPyCu Catalyst.

The aryl-alkyne-modified MWCNTs were prepared by reacting 4-((triisopropylsilyl)ethynyl) benzene-diazonium tetrafluoroborate with purified MWCNTs as previously described.[21] Aryl-alkyne-modified CNTs (30 mg) were dispersed in 30 mL of DMF by sonication for 2 h. Tetrabutylammonium fluoride (1.0 M in THF, 0.2 mL, 0.2 mmol) was added to the solution at 0 °C under an N_2 atmosphere and the solution stirred for 4 h at room temperature. Then, $CuSO_4{\cdot}5H_2O$ (12.0 mg, 0.048 mmol), sodium ascorbate (50 mg, 0.24 mmol), and 2-(azidomethyl)pyridine (150 mg, 0.81 mmol) were added to the solution and the mixture stirred at 50 °C for 48 h under an N_2 atmosphere. The resulting product (CNTs-TAmPy) was collected by filtration and then washed thoroughly with DMF (3×), 50 mmol/L EDTA solution (3×), and ethanol (3×).

The CNTs-TAmPyCu catalyst was prepared by mixing CNTs-TAmPy (20.0 mg) and $CuCl_2$ (40.0 mg) in 10.0 mL of methanol and 10.0 mL of ultrapure water. The solution was stirred at room temperature for 24 h and filtered. The resultant composite was washed using deionized water (3×) and methanol (3×) and then dried under vacuum overnight.

The control sample {CNTs+TAmPyCu} was prepared by mixing MWCNTs (10 mg) with TAmPyCu (1.0 mg) in CH_3CN, and the suspension solution was stirred for 16 h at room temperature. The {CNTs+TAmPyCu} was obtained by centrifugation and dried under vacuum.

Synthesis of the rGO-TAmPyCu Catalyst.

The purified GO (40 mg) and 4-((triisopropylsilyl)ethynyl) benzene-diazonium tetrafluoroborate (200 mg, 0.73 mmol) were dispersed in 40 mL of deionized water under magnetic stirring, and hydrazine hydrate (80%, 1.0 mL, ~16 mmol) was then added. The solution was stirred at 80 °C overnight. After cooling to room temperature, the solution was centrifuged, and the resultant sediment was washed with deionized water (3×) and methanol (CH_3OH, 3×) under sonication and then replaced by DMF. The resulting Phenyl-alkyne-modified rGO was then dispersed in 40 mL of DMF by sonication. Tetrabutylammonium fluoride (1.0 M in THF, 0.1 mL, 0.1 mmol) was added to the solution at 0 ℃ under N_2 atmosphere, and the solution was warmed up to room temperature and further stirred for 3 h. Then $CuSO_4{\cdot}5H_2O$ (6.0 mg, 0.024 mmol), sodium ascorbate (25 mg, 0.12 mmol), and 2-methyl azidopyridine (83 mg, 0.62 mmol) were added to the solution, and the mixture was stirred at 50 ℃ for 36 h under N_2 atmosphere. The resulting product (rGO-TAmPy) was collected by centrifugation and then thoroughly washed with DMF (3×), 50 mmol/L EDTA solution (3×), deionized water (3×) and methanol (3×).

In order to improve the dispersity of the as-prepared rGO-TAmPy, TiO_2 nanoparticles (5.0 mg) was mixed with rGO-TAmPy (10.0 mg) in 20 mL of methanol with sonication, to which $CuCl_2$ (20 mg) was then added. The solution was stirred at room temperature for 24 h and centrifuged. The prepared rGO-TAmPyCu composite was thoroughly washed by deionized water (3×), methanol (3×), and then dried under vacuum.

The control sample {rGO+TAmPyCu} was prepared by mixing rGO (10 mg) with TAmPyCu (1.0 mg) in CH_3CN, and the suspension solution was stirred for 16 h at room temperature. The {rGO+TAmPyCu} was obtained by centrifugation and dried under vacuum.

Catalyst Characterization.

The morphology of CNTs-TAmPyCu/rGO-TAmPyCu was examined using TEM (JEOL JEM-2011) operating at 100 kV. XPS data were collected on a Thermo Escalab 250 XPS instrument with a monochromatic Al Kα X-ray source ($h\nu$ = 1486.6 eV). All binding energies were referenced to the C1s peak (284.6 eV) arising from adventitious carbon. Raman spectra were collected on a confocal microscopy Raman spectrometer (Renishaw, RM-1000) with a laser excitation wavelength of 532 nm. FTIR spectra were recorded on a Shimadzu Fourier transform infrared spectrometer (IRPrestige-21).

Electrochemical Experiment.

The catalyst ink was prepared as follows. The catalyst (10.0 mg) were mixed in a glass vial with a 5 wt% dispersion solution of Nafion (50 µL, Aldrich) and isopropanol (450 µL). The ink was sonicated in a bath sonicator for 2 h. The catalyst ink (10 µL) was applied to the surface of a glassy carbon disk (0.196 cm^2), and the solvent evaporated at room temperature under air to produce a uniform film with a catalyst loading of about 1.0 mg cm^{-2}. Commercial 20 wt% Pt/C on Vulcan XC72R carbon (Johnson Matthey) was used as the reference catalyst.

A rotating ring-disk electrode (RRDE) (Pine Instruments) with a 5.0-mm-diameter glassy carbon disk and Pt ring (geometric area 0.110 cm^{-2}) was used to evaluate the catalyst performance on a CH Instrument Model 760D potentiostat in a standard three-electrode cell. To avoid any potential contamination of the catalyst by Pt, a graphite rod was used as the counter electrode. A Hg/HgO electrode was used as the reference electrode in a 0.1 M KOH electrolyte. All cyclic voltammetry (CV) and RRDE tests were performed at room temperature with a scan rate of 10 mVs^{-1}. The electrolyte was bubbled with O_2 for 30 min prior to each experiment, and O_2 purging was maintained over the electrolyte during the electrochemical measurements. A 20-s potential hold at the open cell potential preceded every polarization experiment.

Results and Discussion

Synthesis and characterization of the CNTs-TAmPyCu and rGO-TAmPyCu catalysts

The TAmPy-grafted CNTs/rGO were prepared in two steps following a similar method as previously reported.[21] A protected aryl-alkyne monolayer was first grafted onto the CNTs/rGO by reacting with triisopropylsilyl (TIPS)-protected ethynyl aryldiazonium. During the process of alkyne functionalization, the GO was reduced by the presented hydrazine at the same time, thus affording the aryl-alkyne modified rGO. Then, de-protecting the TIPS group in situ afforded a grafted reactive ethynyl aryl, which further reacted with 2-(azidomethyl)pyridine through a typical "click" chemistry reaction to produce the triazole-pyridine grafted CNTs/rGO.

The TAmPy functionalized CNTs (CNTs-TAmPy) were characterized by various spectroscopic methods. The FTIR spectrum of CNTs-TAmPy displayed new signals at 1096, 1154, 1210, 1443, and 1580 cm^{-1} compared with the pristine MWCNTs (Figure 2A), among which the signals at 1096 and 1443 cm^{-1} were assignable to stretching vibrations of the triazole ring;[21,22,28] the remaining additional peaks were attributable to vibrations of the pyridine ring. The Raman spectrum of CNTs-TAmPy displayed D and G bands at 1343 and 1584 cm^{-1}, respectively. The D/G band intensity ratio for CNTs-TAmPy (I_D/I_G = 1.18) was higher than that of the pristine MWCNTs (I_D/I_G = 1.07, Figure 2B), suggesting additional defects were formed on the surface of the MWCNTs after covalent modification with the TAmPy ligand. This observation agrees well with previously reported covalent-grafted CNTs.[21, 29] The XPS survey spectrum of CNTs-TAmPy revealed the successful incorporation of nitrogen atoms onto the CNTs with a nitrogen content of 4.58 at% (Figure 2C). The XP N_{1s} spectrum showed a broad nitrogen signal that is deconvoluted into three peaks with binding energies (BEs) of 398.2, 400.0, and 401.1 eV (Figure 2D). The N_{1s} peak at 398.2 eV was assignable to the nitrogen atom of the pyridine group [30] and the peaks at 400.0 and 401.1 eV were attributed to the nitrogen atoms of the triazole ring.[21,28] Consequently, all the spectroscopic characterization results indicated that a triazole-pyridine functional group was successfully grafted onto the surface of MWCNTs.

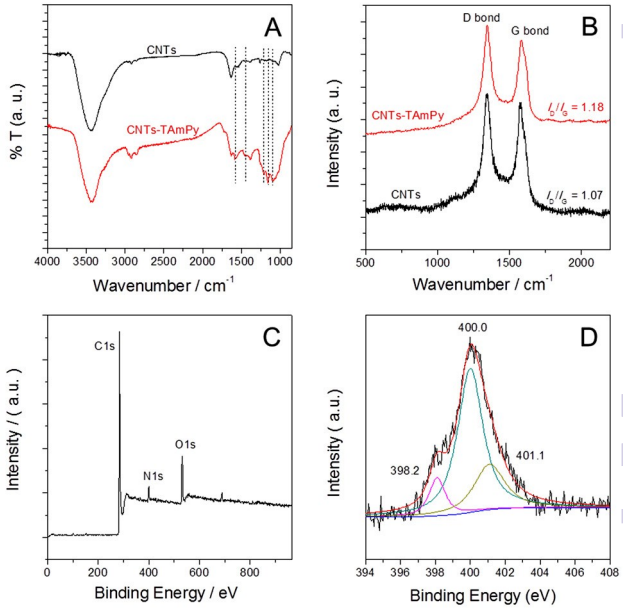

Figure 2 (A) FT-IR spectra of CNTs-TAmPy and MWCNTs. (B) Raman spectra of CNTs-TAmPy and pristine MWCNTs. Excitation = 532 nm. (C) XPS survey spectrum of CNTs-TAmPy. (D) High resolution XP N_{1s} spectrum of CNTs-TAmPy.

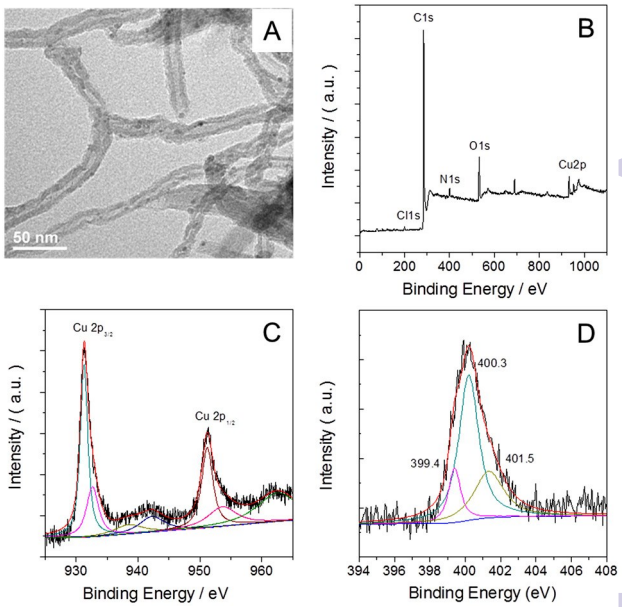

Figure 3 (A) TEM image of CNTs-TAmPyCu. (B) XPS survey spectrum of CNTs-TAmPyCu. (C) High resolution XP Cu2P spectrum of CNTs-TAmPyCu. (D) High resolution XP N1s spectrum of CNTs-TAmPyCu.

Coordination of copper ions with the triazole-pyridine-functionalized CNTs produced the CNTs-TAmPyCu catalyst. The morphology of the CNTs-TAmPyCu was examined using transmission electron microscopy (TEM, Figure 3A), which revealed that it maintained the morphology of the individual nanotubes and

had a length of about 2.0 μm. The XPS survey spectrum of the CNTs-TAmPyCu showed signatures of carbon, nitrogen, oxygen, chlorine, and copper (Figure 3B). The copper content was determined to be 0.94 at% by XPS analysis. The Cu_{2p} core level XP spectrum displayed peaks at 931.3 and 951.2 eV, which were assigned to the BE values of $Cu_{2p3/2}$ and $Cu_{2p1/2}$, respectively (Figure 3C).[31-34] Broad Cu(II) satellite peaks at 940–947 and 960–967 eV were also presented. The N_{1s} XP spectrum of the CNTs-TAmPyCu showed a broad nitrogen signal that was deconvoluted into three peaks with BE at 399.4, 400.3, and 401.5 eV (Figure 3D). After Cu incorporation, the binding energies assignable to the pyridine-N (399.4 eV) and the triazole-N (400.3, 401.5 eV) with the CNTs-TAmPyCu catalyst displayed up-shifts relative to those of the un-coordinated CNTs-TAmPy (pyridine-N: 398.2 eV; triazole-N: 400.0, 401.1 eV). This suggests the coordination of the triazole-pyrdine TAmPy ligand with Cu ions. The N-to-Cu ratio of about 4 indicates the overall covalent-attached TAmPy ligands most probably coordinate with Cu ions in a 1:1 ratio, as suggested in Figure 1.

Compared to GO, the FTIR spectra of rGO-TAmPy shows additional signals at 1409 and 1096 cm^{-1} which were assignable to stretching vibrations of a triazole ring (Figure 4A).[21, 22, 28] The Raman spectrum of rGO-TAmPy displayed D and G bands at 1347 and 1589 cm^{-1}, respectively. The D/G band intensity ratio for rGO-TAmPy (I_D/I_G = 1.19) was higher than that of GO (I_D/I_G = 0.97, Figure 4B), which indicates that more defects were created on the surface of the GO after covalent grafting.[35-37] The XPS survey spectrum of rGO-TAmPy showed signatures of carbon, nitrogen, and oxygen (Figure 4C). The N1s XP spectral of rGO-TAmPy showed a broad nitrogen signal that can be deconvoluted into three components with binding energies of 399.2 eV, 400.3 eV and 401.3 eV (Figure 4D). The N1s peaks at 399.2 eV is assigned to the pyridine-N, another two peaks are attributed to the triazole-N. The nitrogen content is measured to be 4.47 at%. Thus, all the spectroscopic evidence suggested the successful grafting of a TAmPy ligand on rGO.

Coordination of copper ions with the triazole-pyridine-functionalized rGO produced the rGO-TAmPyCu catalyst. The TEM image of rGO-TAmPyCu revealed the lamellar morphology, where the TiO_2 nanoparticles that used for preventing re-stacking of rGO were scatter on the graphene surface (Figure 5A). The XPS survey spectrum of rGO-TAmPyCu showed signatures of carbon, nitrogen, oxygen, chlorine, titanium, and copper (Figure 5B), and the copper content was determined to be 0.95 at%. The Cu2p core-level XP spectrum displayed two major peaks at 930-937 eV and 950-956 eV (Figure 5C), similar to that observed with the CNTs-TAmPyCu catalyst. The N1s XP spectrum of the rGO-TAmPyCu showed a broad nitrogen signal that can be deconvoluted into three components with binding energies of 399.3 eV, 400.5 eV and 401.6 eV (Figure 5D), which showed up-shifts compared to that of the rGO-TAmPy.

ORR Electrocatalytic Activity

Cyclic voltammetry (CV) performed with the CNTs-TAmPyCu-modified GC electrode in an O_2-saturated 0.10 M KOH solution revealed that the CNTs-TAmPyCu catalyst was electrochemically active toward O_2 with a well-defined reduction wave at a formal potential of *ca.* −0.20 V *vs.* Hg/HgO (Figure 6A). However, the simple mixture {CNTs+TAmPyCu} (−0.23 V, Figure S1) and pristine CNTs (−0.30 V, Figure S2) showed negative shifts of potential for O_2 reduction compared with the CNTs-TAmPyCu catalyst. The cyclic voltammogram of the rGO-TAmPyCu catalyst showed O_2 reduction wave at the same potential as that of CNTs-TAmPyCu (Figure 7A).

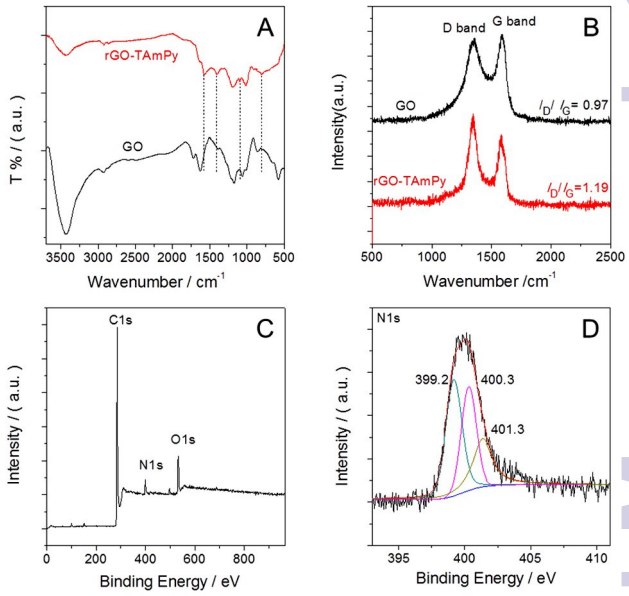

Figure 4 (A) FTIR spectra of GO, and rGO-TAmPy. (B) Raman spectra of GO (black), and rGO-TADPy (red). Excitation = 532 nm. (C) XPS survey spectrum of rGO-TAmPy. (D) High resolution XP N1s spectrum of rGO-TAmPy.

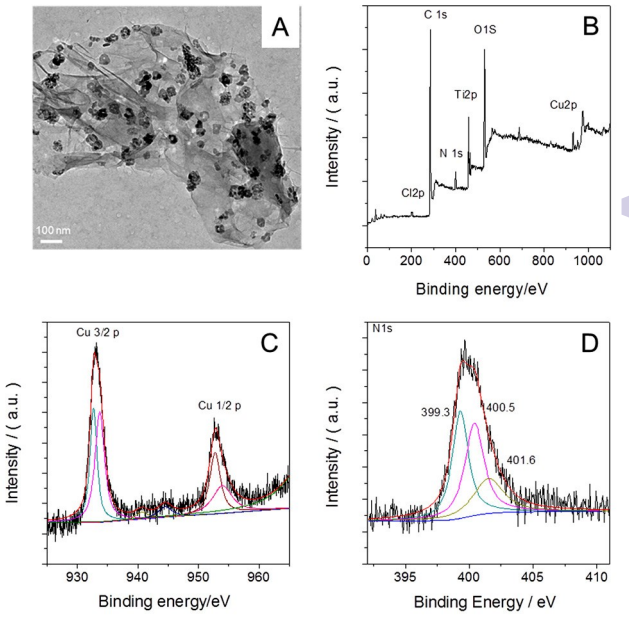

Figure 5 (A) TEM image of rGO-TAmPyCu (B) XPS survey spectrum of rGO-TAmPyCu. (C) High resolution XP Cu2P spectrum of rGO-TAmPyCu. (D) High resolution XP N1s spectrum of rGO-TAmPyCu.

A rotating-disk electrode was employed to investigate the ORR pathway for the catalysts in 0.1 M KOH solution at room temperature. Figure 6B displays the ORR polarization curves with CNTs-TAmPyCu, {CNTs+TAmPyCu} (a simple mixture of pristine CNTs and the TAmPyCu complex), and pristine

CNTs catalysts. The half-wave potential ($E_{1/2}$) was usually taken for estimating the electrocatalytic activity of catalysts in a mixed kinetic/diffusion region. The $E_{1/2}$ value of CNTs-TAmPyCu was −0.21 V, which was much higher than that of the {CNTs+TAmPyCu} (−0.29 V) and CNTs (−0.30 V) catalysts. While for the graphene grafted rGO-TAmPyCu catalyst, it demonstrated the same ORR half-wave potential as the CNTs-TAmPyCu catalyst ($E_{1/2}$ = −0.21 V, Figure 6B), and the $E_{1/2}$ value is more positive than that of the physisorbed {rGO+TAmPyCu} ($E_{1/2}$ = −0.29 V, Table 1, Figure S4). Moreover, both of the covalently grafted catalysts showed a significant increase of limiting current density relative to the pristine CNTs and rGO, respectively. Under similar experimental conditions, the $E_{1/2}$ value of about -0.10 V was obtained for the Pt/C catalyst (Figure 7B). Consequently, these results clearly verified that covalent immobilization of copper complex on the surface of CNTs/rGO significantly reduces the ORR overpotential compared to their physisorbed counterparts.

Rotating-disk voltammograms of the CNTs-TAmPyCu/rGO-TAmPyCu catalysts at different rotation rates are shown in Figure 6C and 7C, and its rotation-rate-dependent current–potential curves are depicted in Figure 6D and 7D, respectively. Koutecky–Levich plots at various potentials exhibited good linearity. The electron transfer number (n) was calculated to be around 3.50 for the CNTs-TAmPyCu catalyst in the potential range from −0.35 to −0.60 V by the slopes of the Koutecky–Levich plots.[38] It is worth to note that under similar experimental conditions, the value of electron transfer number was calculated as high as 3.82 for the graphene grafted rGO-TAmPyCu catalyst, suggesting a close 4e$^-$ oxygen reduction process.

The RRDE was further employed to compare the ORR electrocatalytic activity of different samples. The partially 2e$^-$ reduced product hydroperoxide ($^-HO_2$) can be detected from the ring electrode. Figure 6 E and 7E depicted the results of peroxide generated by different samples, respectively. It is evidently shown that the yields of peroxide generated from the covalently grafted catalysts CNTs-TAmPyCu/rGO-TAmPyCu were remarkably lower than that of their physisorbed counterparts (Table 1), suggesting the grafted catalyst has a higher selectivity of 4e$^-$ versus 2e$^-$ reduction of O_2. This could be explained by the fact that the covalently arranged two proximal Cu sites on the surface of supporting, where O_2 bridges two Cu sites as suggested previously,[15-18] might promote more efficient O_2 reduction than that of the physisorbed discrete single Cu site.

It is noteworthy that the rGO-TAmPyCu catalyst generated much less amount of peroxide (~ 9%) compared to that of the CNTs-TAmPyCu catalyst (~ 19%). Under similar grafted Cu density that was analysed by XPS analysis, the rGO-TAmPyCu and CNTs-TAmPyCu catalysts showed almost the same ORR half-wave and onset potentials, while the rGO-TAmPyCu catalyst significantly enhances the selectivity of 4e$^-$ reduction of O_2 relative to the CNTs-TAmPyCu catalyst. This phenomenon may reflect the effect of different catalyst supporting. It is anticipated that for the same surface distance, the spatial distance between two neighbor Cu sites on the planar rGO is much shorter than that on the tubular CNTs. Thus, the graphene grafted catalyst rGO-TAmPyCu may produce more formal adjacently arranged Cu sites than that of the CNTs grafted CNTs-TAmPyCu catalyst, which might contribute to the enhanced 4e$^-$ reduction process. It is interesting to note that a graphene covalently grafted multinuclear Cu assembly, rGO-TADPyCu,[22] displayed much more positive ORR half-wave and onset potentials than the rGO-TAmPyCu catalyst (Table 1). These results clearly indicate that proximal dinuclear Cu sites significantly promote the oxygen 4e$^-$ reduction process, and a multinuclear Cu assembly further effectively lowers the ORR overpotential.

Table 1 ORR activity of the catalysts [a]

Catalyst	[b]E_{onset}	[c]$E_{1/2}$	H_2O_2% [d]	n [d]
{CNTs+TAmPyCu}	-0.076	-0.29	42%	3.18
CNTs-TAmPyCu	-0.045	-0.21	19%	3.50
{rGO+TAmPyCu}	-0.071	-0.29	47%	3.20
rGO-TAmPyCu	-0.044	-0.21	9%	3.82
rGO-TADPyCu [e]	-0.019	-0.185	8%	3.85

[a] Electrochemical evaluation was performed in a 0.1 M KOH solution. Catalyst loading: 1.0 mg/cm^{-2}. Potential was reported in V vs. Hg/HgO. [b] The E_{onset} is defined as the potential where the current deviates from that of the background under Ar atmosphere. [c] The $E_{1/2}$ was obtained from the LSV under 1600 rpm. [d] The value was taken at potential of -0.35 V vs. Hg/HgO. [e] A multinuclear assembly on rGO from ref. 22.

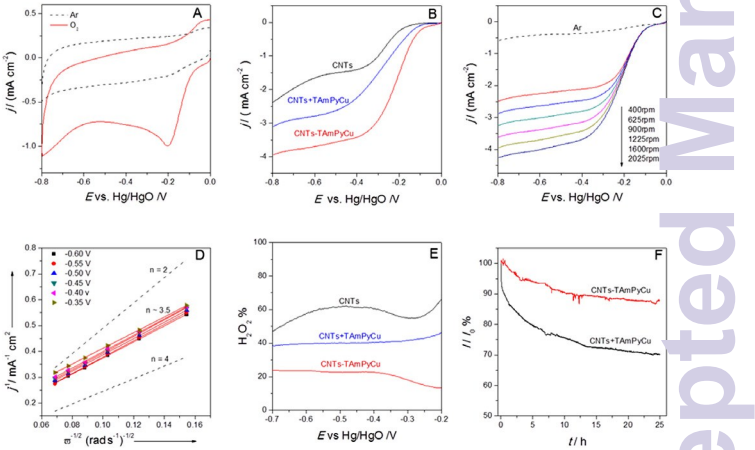

Figure 6 (A) Cyclic voltammograms of CNTs-TAmPyCu in 0.1 M KOH solution saturated with Ar (black line) and O_2 (red line), respectively. (B) LSV curves of CNTs (black), {CNTs+TamPyCu} (blue), and CNTs-TAmPyCu (red) in O_2-saturated 0.1 M KOH solution at 1600 rpm. (C) Rotating-disk voltammograms of CNTs-TAmPyCu in O_2-saturated 0.1 M KOH solution at the different rotation rates indicated. The dotted line indicates the background when scanned in Ar-saturated solution. (D) Koutecky–Levich plots of CNTs-TAmPyCu derived from RDE measurements at different potentials. Theoretical 2e$^-$ and 4e$^-$ reduction processes are shown as dotted lines. (E) Peroxide yield for CNTs (black), {CNTs+TamPyCu} (blue), and CNTs-TAmPyCu (red) catalysts. (F) Current–time (*i*–*t*) chronoamperometric response of CNTs-TAmPyCu (red), and {CNTs+TamPyCu} (black) modified GC electrode at −0.4 V in an O_2-saturated 0.1 M KOH solution.

The stability of the catalysts was tested by chronoamperometric measurements, and the results are shown in Figure 6F and 7F, respectively. The covalently grafted CNTs-TAmPyCu/rGO-TAmPyCu catalysts maintained above 85% of its initial current after 25 h, while the physisorbed counterparts retained less than 70% of the initial current. These results signified that the CNTs-TAmPyCu/rGO-TAmPyCu catalysts have improved stability over the physisorbed composites {CNTs/rGO+TamPyCu}, and also better than the Pt/C catalyst (Figure 7F) in 0.1 M KOH solution. The enhanced catalyst stability might benefit from both their relatively high selectivity of 4e$^-$ versus the 2e$^-$ reduction of dioxygen and the covalent grafting of the catalyst onto the surface of the supporting materials. A methanol crossover test on the CNTs-TAmPyCu/rGO-TAmPyCu catalysts was also performed. As is usual for other non-precious-metal catalysts, both catalysts demonstrated good tolerance to the methanol crossover effect. It showed a stable amperometric response after the addition of

2.0 M methanol, which is better than that of commercial Pt/C catalysts (Figure S5, S6).

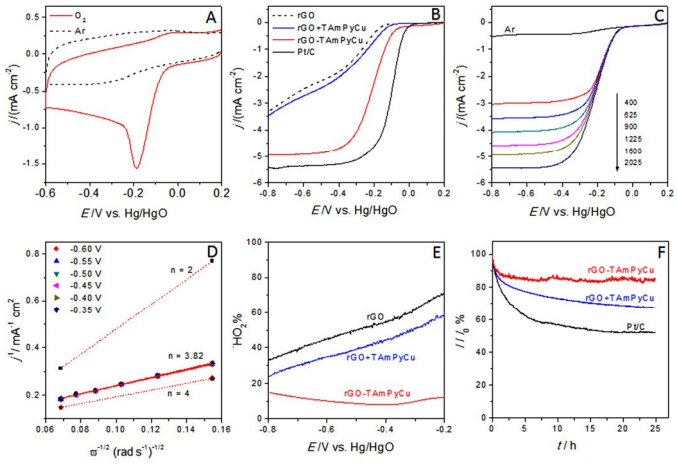

Figure 7 (A) Cyclic voltammograms of rGO-TAmPyCu in 0.1 M KOH solution saturated with O_2 (black line) and Ar (red line), respectively. (B) LSV curves of rGO (dotted black), {rGO+TamPyCu} (blue), rGO-TAmPyCu (red) and 20% Pt/C (black) in O_2-saturated 0.1 M KOH solution at 1600 rpm. (C) Rotating-disk voltammograms of rGO-TAmPyCu in O_2-saturated 0.1 M KOH solution at the different rotation rates indicated. The dotted line indicates the background when scanned in Ar-saturated solution. (D) Koutecky–Levich plots of rGO-TAmPyCu derived from RDE measurements at different potentials. Theoretical $2e^-$ and $4e^-$ reduction processes are shown as dotted lines. (E) Peroxide yield for rGO (black), {rGO+TamPyCu} (blue), and rGO-TAmPyCu (red) catalysts. (F) Current–time (*i*–*t*) chronoamperometric response of rGO-TAmPyCu (red), {rGO+TamPyCu} (blue) and Pt/C (black) modified GC electrode at −0.4 V in an O_2-saturated 0.1 M KOH solution.

Conclusions

In summary, a triazole-pyridine ligand (TAmPy) was covalent grafted onto the surface of MWCNTs and rGO, respectively. Coordination of copper ions afforded new Cu-complex-based ORR catalysts with relative high ORR activity and stability. Covalent immobilization of the copper complex on these carbon based supporting materials endowed the corresponding CNTs-TAmPyCu and rGO-TamPyCu catalysts with much higher ORR activity and improved stability than that of their physisorbed counterparts. The experimental results also revealed the effect of different catalyst supporting on the ORR activity of the Cu catalysts. Copper complex covalently immobilized on flat rGO demonstrated much higher selectivity of $4e^-$ reduction of O_2 than that on the tubular CNTs. The experimental results suggest that proximal dinuclear Cu sites on supporting material effectively promote the oxygen $4e^-$ reduction process, and a multinuclear Cu assembly further impressively lowers the ORR overpotential. This study offers a non-pyrolyzed approach for covalent immobilization of non-precious-metal ORR catalysts on carbon-based materials (CNTs/rGO) with high ORR activity while their chemical structures are well defined. This will make it possible to tune ORR activity further through ligand design.

Acknowledgements

This study was financially supported by the NSF of China (no 21271072), the Program for Professor of Special Appointment (Eastern Scholar) at Shanghai Institutions of Higher Learning, and sponsored by Shanghai Pujiang Program (no. 13J1401900).

Notes and references

[a] *Department of Chemistry, East China University of Science and Technology, Shanghai, 200237, P. R. China,* E-mail: liujingang@ecust.edu.cn

†Electronic Supplementary Information (ESI) available: additional figures. See DOI: 10.1039/b000000x/

1 M. K. Debe, *Nature*. 2012, **486**, 43 .
2 F. Chen and J. Chen, *Chem. Soc. Rev.* 2012, **41**, 2172.
3 R. L. Liu, D. Q. Wu, X. L. Feng and K. Müllen, *Angew. Chem. Int. Ed.* 2010, **122**, 2619.
4 A. Topalov, I. Katsounaros, M. Auinger, S. Cherevko, J. Meier, S. Klemm and K. Mayrhofer, *Angew. Chem. Int. Ed.* 2012, **51**, 12613.
5 M. Nesselberger, M. Roefzaad, R. Hamou, P. Biedermann, F. Schweinberger, S. Kunz, K. Schloegl, G. Wiberg, S. Ashton, U. Heiz, K. J. J. Mayrhofer and M. Arenz, *Nat. Mater*. 2013, **12**, 919.
6 Z. Chen, D. Higgins, A. Yu, L. Zhang and J. Zhang, *Energy & Environ Sci*. 2011, **4,** 3167.
7 Y. Zheng, Y. Jiao, M. Jaroniec, Y. Jin and S. Z. Qiao, *Small* 2012, **8** 3550.
8 J. A. Cracknell, K. A. Vincent and F. A. Armstrong, *Chem. Rev.* 2008, **108,** 2439.
9 G. Wu, K. L. More, C. M. Johnston and P. Zelenay, *Science* 2011, **332**, 443.
10 M. Lefèvre, E. Proietti, F. Jaouen and J.-P. Dodelet, *Science* 2009, **324,** 71.
11 N. Ramaswamy, U. Tylus, Q. Jia and S. Mukerjee, *J. Am. Chem. Soc.* 2013, **135**, 15443.
12 N. Mano, J. L. Fernandez, Y. Kim, W. Shin, A. J. Bard and A. Heller, *J. Am. Chem. Soc.* 2003, **125,** 15290.
13 M. A. Thorseth, C. E. Tornow, E. C.M. Tse and A. A. Gewirth, *Coord. Chem. Rev.* 2013, **257,** 130.
14 C. X. Cai, K. H. Xue, X. Y. Xu and Q. H. Luo, *J. Appl. Electrochem.* 1997, **27**, 793.
15 Y. Lei and F. C. Anson, *Inorg. Chem.* 1995, **34**, 1083.
16 J. Zhang and F. C. Anson, *J. Electroanal. Chem.* 1993, **348,** 81.
17 C. C. L. McCrory, X. Ottenwaelder, T. D. P. Stack and C. E. D. Chidsey, *J. Phys. Chem. A* 2007, **111**, 12641.
18 C. C. L. McCrory, A. Devadoss, X. Ottenwaelder, R. D. Lowe, T. D. P. Stack and C. E. D. Chidsey, *J. Am. Chem. Soc.* 2011, **133,** 3696.
19 M. S. Thorum, J. Yadav and A. A. Gewirth, *Angew. Chem. Int. Ed.* 2009, **48,** 165.
20 F. R. Brushett, M. S. Thorum, N. S. Lioutas, M. S. Naughton, C Toron, H.-R. M. Jhong, A. A. Gewirth and P. J. A. Kenis, *J. Am. Chem. Soc.* 2010, **132,** 12185.
21 P.-J. Wei, G.-Q. Yu, Y. Naruta and J.-G. Liu, *Angew. Chem. Int. Ed.* 2014, **53,** 6659.
22 Y.-T. Xi, P.-J. Wei, R.-C. Wang and J.-G. Liu, *Chem. Commun.* **2015** *51*, 7455.
23 N. I. Kovtyukhova, P. J. Ollivier, B. R. Martin, T. E. Mallouk, S. A Chizhik, E. V. Buzaneva and A. D. Gorchinskiy, *Chem. Mater.* 1999, **11**, 771.
24 W. S. Hummers and R. E. Offeman, *J. Am. Chem. Soc.* 1958, **80**, 1339.
25 Y. R. Leroux, H. Fei, J.-M. Noel, C. Roux and P. Hapiot, *J. Am. Chem. Soc.* 2010, **132**, 14039.
26 J. Ritschel, F. Sasse and M. E. Maier, *Eur. J. Org. Chem.* 2007, **1,** 78.
27 D. Urankar, B. Pinter, A. Pevec, F. D. Proft, I. Turel and J. Kosmrlj, *Inorg. Chem.* 2010, **49,** 4820.
28 H.-X. Wang, K.-G. Zhou, Y.-L. Xie, J. Zeng, N.-N. Chai, J. Li and H.-L. Zhang, *Chem. Commun.* 2011, **47**, 5747.
29 C. Gao. Y. Jin. H. Kong. R. L. D.Whitby, S. F. A. Acquah, G. Y Chen, H. Qian, A. Hartschuh, S. R. P. Silva, S. Henley, P. Fearon, H. W. Kroto and D. R. M. Walton, *J. Phys. Chem. B.* 2005, **109**, 11925.
30 A. Gölzhäuser, S. Panov, M. Mast, A. Schertel, M. Grunze and Wöll, *Surf. Sci.* 1995, **334**, 235.
31 J. Mao, L. Yang, P. Yu, X. Wei and L. Mao, *Electrochem. Commun.* 2012, **19**, 29.
32 X. Qing, J. Shi, C. Ma, M. Fan, Z. Bai, Z. Chen, J. Qiao and J. Zha g, *J. Power Sources* 2014, **266**, 88.

33 T. Waechtler, S. Oswald, N. Roth, A. Jakob, H. Lang, R. E. E. Schulz, T. Gessner, A. Moskvinova, S. Schulze and M. Hietschold, *J. Electrochem. Soc.* 2009, **156**, H453.
34 E. Moretti, M. Lenarda, P. Riello, L. Storaro, A. Talon, R. Frattina, A. Reyes-Carmona, A. Jiménez-López and E. Rodríguez-Castellón, *Appl. Catal. B: Environ.* 2013, **129**, 556.
35 D. S. Sutar, P. K. Narayanam, G. Singh, V. D. Botcha, S. S. Talwar, R. S. Srinivasa and S. S. Major, *Thin Solid Films* 2012, **520,** 5991–5996.
36 A. Ganguly, S. Sharma, P. Papakonstantinou and J. Hamilton, *J. Phys. Chem. C.* 2011, **115**, 17009.
37 Z. J. Fan, K. Wang, T. Wei, J. Yan, L. P. Song and B. Shao, *Carbon* 2010, **48**, 1686.
38 A. J. Bard and L. R. Faulken, *Electrochemical Methods: Fundamental and Applications*, 2nd ed., Wiley-VCH, New York, 2001.